Friction

Research Article

Energy analysis of contact nonlinear transitions: Insights on the origin of limit cycles and bi-stable states in friction-induced instabilities

Matteo Cattai[1,✉], Davide Tonazzi[1], Simone Ciprari[1,2,3], Francesco Massi[1]

Cite this article: Cattai M, Tonazzi D, Ciprari S, et al. *Friction* 2026, **14**(6): 9441215. https://doi.org/10.26599/FRICT.2026.9441215

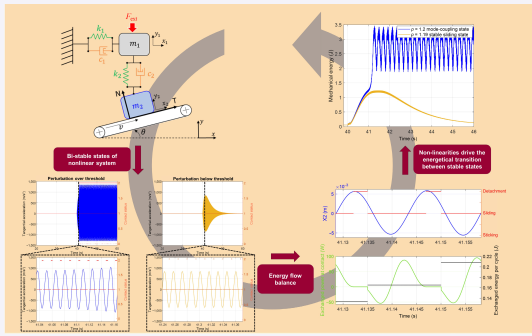

ABSTRACT: This work explores the bi-stable behavior of a frictional system susceptible to mode-coupling instability. The focus is placed on the variations of the energy flows at the contact, due to external perturbations, and the role of contact nonlinearities on the system dynamic response. A lumped parameter numerical model, incorporating contact nonlinearities, is developed, allowing transitions between sliding, sticking, and detachment contact conditions. While prestressed complex eigenvalue analysis (CEA) allows for the identification of instabilities in the linearized frictional system, transient simulations were conducted to investigate the nonlinear system dynamics and the possibility of switching between two stable states (mode coupling or stable sliding) by an external perturbation. The investigation of the bi-stable state has been carried out by performing an energy balance of the system, accounting for the exchanged mechanical energies at the contact, to highlight the key role of contact nonlinearities in driving the power flows at the origin of the different stable states and respective limit cycle. The findings underscore the critical role of contact nonlinearities in shaping the power flows at the contact interface, determining the transition between stable sliding and mode-coupling, and providing further insights into the "fugitive" feature of mode-coupling instabilities.

KEYWORDS: sliding friction; non-linear dynamics; contact instability; bi-stable response; energy approach

1 Introduction

Friction-induced vibrations (FIVs) are a phenomenon of interest in various engineering fields, consisting of the generation of mechanical oscillations due to the interaction between contacting surfaces in relative motion. Although FIVs are an ever-present phenomenon whenever bodies in relative motion interact [1], unstable FIVs [2, 3] are considered a major problem, both in dry [4, 5] and lubricated [6] contacts, since they are responsible for noise [7, 8], discomfort, and exacerbated wear [9, 10]. As an example, in the automotive industry [11], squeal, groan noise, and other noise vibration harshness (NVH) issues [12] often result from the frictional contact occurring in brakes and clutches [13–15]. These phenomena lead to replacement costs sustained by the brake manufacturers.

Contact instabilities can be attributed to various factors, such as the dependence of the friction coefficient on relative velocity [16–18] or mode coupling [19] due to a flutter-like instability, which arises even for constant values of the friction coefficient [20–22]. Energy analyses showed how, during the rise of the instability, the energy is transferred by friction to unstable modes of the system [23, 24], increasing the amplitude of vibrations exponentially up to a limit cycle. Friction coefficient has been found to be one of the fundamental parameters for the stability of the system [25–27], as well as contact nonlinearities, which play a crucial role in the onset of instabilities [28]. Specifically, they alter the energy flows at the contact, enabling the system to accumulate the energy required for the initiation of an unstable response. Furthermore, experimental [29] and finite element [30–32] analyses pointed out their fundamental role in governing the transition from the exponential growth of vibration amplitude to the stable behavior at the limit cycle, highlighting that their contribution to the energy exchanges at the contact significantly affects both the oscillation amplitude and frequency [33].

For the characterization of the phenomenon, both experimental and numerical approaches have been used in the literature [34]. While experimental tests are influenced by the intrinsic complex nature of contact systems, making it difficult to decouple the effects of single parameters on the dynamic response of the system, they have often been used to compare real application

[1] DIMA-Department of Mechanical and Aerospace Engineering, Sapienza University of Rome, Roma 00185, Italy. [2] LaMCoS, INSA Lyon, CNRS, UMR5259, Villeurbanne 69621, France. [3] Safran Landing Systems, Villeurbanne 69100, France.

✉ Corresponding author. E-mail: matteo.cattai@uniroma1.it

Received: July 28, 2025; Revised: September 30, 2025; Accepted: January 5, 2026

results to fundamental or numerical analyses [35, 36]. On the other hand, considering numerical analyses, transient simulations reproducing the true geometry of the system require a significant amount of computational effort and time [37], needing often for a simplification of the system or the contact itself. Hence, to study the dynamic response of the system, complex eigenvalues analyses (CEA) are usually performed [21, 25] linearizing the system around the equilibrium sliding state. This type of analysis returns the complex eigenvalues of the system as a function of design parameters. To determine the behavior of the system, the sign of the real part of the eigenvalues is observed: A positive value, in fact, leads to an exponential increase in amplitude of vibration of the respective mode. This unstable state of the system dynamics leads to an increase of system oscillations, up to a second stable state characterized by a limit cycle, where nonlinearities limit the vibration amplitude. Consequently, the stable state at the limit cycle cannot be predicted by the CEA, which is intrinsically linear. Previous results in literature highlighted how CEA is not sufficient to fully describe the system behavior, since non-linear phenomena arise at the contact, such as local sticking or detachment, altering the dynamics and the response of the system [37, 38], which needs to be further investigated. Previous works in literature showed as well how the CEA linear analysis overpredicts the number of unstable modes of the system [21, 25, 38].

Moreover, because of nonlinearities, when considering contact instabilities, both experimental and numerical results in the literature have demonstrated the presence of a subcritical bifurcation associated with underpredicted modes [21, 39, 40]. Specifically, the system exhibits bi-stable behavior, where it can switch between two possible attractors in response to a sufficient external perturbation [26, 35, 41]. Recent literature has not only examined the possibility for dynamical systems to switch between stable states, but has also introduced the concept of basins of attraction as a means to assess the robustness of each state against perturbations [19]. Several studies have shown that, under the same set of parameters, different initial conditions may lead the system to distinct stable periodic oscillations. In this framework, a basin of attraction identifies the set of initial conditions that allow the system to preserve its stable dynamics even in the presence of external disturbances. The larger the basin, the more robust the corresponding state [21, 42].

The original contribution of the present work relies on the investigation of the phenomenological mechanisms leading to the coexistence of multiple stable states in contact systems, by an energy balance and analysis during the system's transient response. To investigate such nonlinear features of dynamic systems, lumped parameter models have been generally used [38, 39], as they enable transient parametric analyses while keeping computational cost low. Various "mass-on-a-moving-belt" numerical models have been employed in literature to simulate contact instabilities, focusing on simple geometries and analysing the effects of system parameters individually [22, 37, 39]. The work presented in this paper adds an original contribution by investigating the variations of the energy flows at the contact interface [43], which are found to play a fundamental role in the transitions between the different dynamic responses of the system.

The analysis proposed in this paper is then developed with a mass on a moving belt model, implementing non-linear contact behaviors, such as sticking and detachment. The model is first developed, then its dynamics in the linear regime is investigated by CEA, followed by a transient analysis simulation of different types of instabilities. The attention is here focused on the mode coupling instability, highlighting the existence of a bi-stable state of the system as a function of the friction coefficient and of an applied external perturbation. A subcritical Hopf's bifurcation is identified, evidencing the occurrence of either a stable sliding state or mode coupling instability under the same boundary conditions. Finally, the role of energy flow modifications, due to contact nonlinearities, on the occurrence and development of mode coupling is investigated, suggesting the energy balance approach as a key framework for the investigation and prediction of bi-stable states under frictional contacts.

Although microscopic dissipation mechanisms at the contact are known to significantly affect the evolution of contact dynamics and local energy exchange [44], the present model considers only macroscopic mechanical effects, focusing on the overall system dynamic response and its nonlinearities due to the switching between sliding, sticking, and detachment status at the contact. Moreover, being interested in the simulation of the mode-coupling mechanical instability, driven by the dynamic response of the system, only macroscopic dissipation phenomena, namely frictional losses at the interface and internal material damping, and only mechanical energy flows are considered, neglecting thermal energy flows.

2 Numerical model

2.1 Model description

The lumped parameters model used for this analysis is presented in Fig. 1. It consists of two masses, m_1 and m_2, connected by a spring-damper system (k_2 and c_2). The mass m_1 is connected with the frame through a second spring-damper system (k_1 and c_1), while the mass m_2 is in frictional contact with a rigid belt, moving with an imposed velocity v. A synchronous motion of the two masses is assumed along the x-axis direction by imposing a rigid connection. Such an assumption allows for the reduction of the degrees of freedom (DOF) of the system to three. In terms of load, the system is subjected to an external vertical force (y-axis direction) in order to put in contact the mass m_2 with the moving belt, which is inclined of an angle θ compared to x, which results in the normal (N) and tangential (T) frictional forces, as reported in Fig. 1. The belt inclination angle allows for coupling the normal and tangential DOF, due to the non-diagonal terms in the system matrixes, caused by the friction terms.

A MATLAB code is used to solve the equations of motion, allowing as well to verify the contact status between the mass m_2 and the moving belt; three different values of the contact states for the mass m_2 are possible: sticking (0), sliding (1), and detachment (2).

The contact status is defined by the following conditions, as a

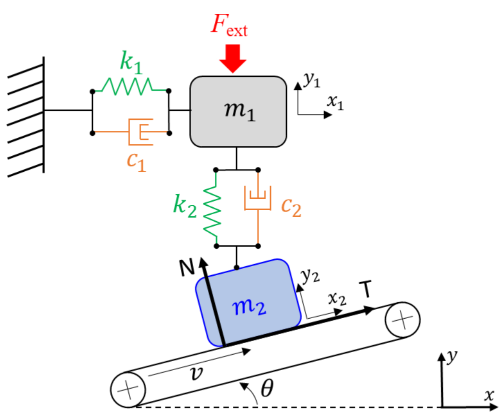

Fig. 1 Lumped parameters model.

function of the contact forces and relative velocity, which are verified at each time step:

• Detachment: If positive $N>0$ and nil normal gap between the belt and the mass m_2 ($y_2=0$) conditions are not both satisfied, the contact mass m_2 results in detachment and the contact status assumes the value 2.

• Contact: If ($N>0$) and ($y_2=0$) are both satisfied, the contact mass m_2 results in contact with the belt. In this case, two conditions can be experienced:

o Sticking: If the relative velocity between the mass and the belt is nil and the condition $T \le \mu_s N$ is satisfied (defining μ_s as the static friction coefficient), the contact results in sticking and the contact status assumes the value 0.

o Sliding: In the remaining case, the contact results in sliding and the contact status assumes the value 1, with the friction force defined as $F=-\mu(v_{\mathrm{rel}})\cdot sign(v_{\mathrm{rel}})\cdot N$.

The friction law used in this work is assumed as shown in Eq. (1):

$$\mu=\mu_{\mathrm{d}}-(\mu_{\mathrm{d}}-\mu_{\mathrm{s}})\exp(-d\cdot|v_{\mathrm{rel}}|) \tag{1}$$

in which μ_s and μ_d represent, respectively, the static and dynamic friction coefficient, while d is the decaying factor, which has been set to 0.5 for all the numerical simulations. More in detail, two types of frictional laws, i.e., a constant friction coefficient law and an exponentially decreasing friction coefficient law, have been used for the present investigation. An example of the used frictional laws is reported in Fig. 2.

Depending on the contact status, the equations of motion and even the number of DOF (in detachment the DOF are 3, in sliding 2, and in sticking they reduce to 1) are different. For this reason, at each time step, the considered equations of motion of the system are modified and solved accordingly. In sliding contact, frictional forces must be considered, and the non-detachment condition $y_2=0$ is imposed. Considering $\boldsymbol{r}$ as the displacement vector, containing the displacements of all DOF, $\boldsymbol{F}$ as the external force vector and defining $\boldsymbol{M}$, $\boldsymbol{C}$, $\boldsymbol{K}$ as the mass, damping and stiffness matrixes, respectively, the resulting equations characterising the dynamics of the system are shown in Eqs. (2) and (3):

$$\boldsymbol{M}\ddot{\boldsymbol{r}}+\boldsymbol{C}\dot{\boldsymbol{r}}+\boldsymbol{K}\boldsymbol{r}=\boldsymbol{F} \tag{2}$$

with

$$\boldsymbol{M}=\begin{bmatrix} m_2+m_1\cos^2\theta+\mu_{\mathrm{d}}m_1\cos\theta\sin\theta & 0 \\ 0 & m_1 \end{bmatrix}$$

$$\boldsymbol{C}=\begin{bmatrix} c_2\sin^2\theta+c_1\cos^2\theta+\mu_{\mathrm{d}}(c_1-c_2)\cos\theta\sin\theta & -c_2\sin\theta+\mu_{\mathrm{d}}c_2\cos\theta \\ -c_2\sin\theta & c_2 \end{bmatrix}$$

$$\boldsymbol{K}=\begin{bmatrix} k_2\sin^2\theta+k_1\cos^2\theta+\frac{\mu_{\mathrm{d}}}{2}(k_1-k_2)\sin 2\theta & -k_2\sin\theta+\mu_{\mathrm{d}}k_2\cos\theta \\ -k_2\sin\theta & k_2 \end{bmatrix}$$

$$\boldsymbol{r}=\begin{pmatrix} x_2 \\ y_1 \end{pmatrix}$$

$$\boldsymbol{F}=\begin{pmatrix} 0 \\ -F_{\mathrm{ext}} \end{pmatrix} \tag{3}$$

In a detachment condition, a third degree of freedom must be considered in the y_2 direction, resulting in Eqs. (4) and (5):

$$\boldsymbol{M}_{\mathrm{D}}\ddot{\boldsymbol{r}}+\boldsymbol{C}_{\mathrm{D}}\dot{\boldsymbol{r}}+\boldsymbol{K}_{\mathrm{D}}\boldsymbol{r}=\boldsymbol{F} \tag{4}$$

with

$$\boldsymbol{M}_{\mathrm{D}}=\begin{bmatrix} m_1\cos^2\theta+m_2 & 0 & -m_1\sin\theta\cos\theta \\ 0 & m_1 & 0 \\ -m_1\cos\theta\sin\theta & 0 & m_1\sin^2\theta+m_2 \end{bmatrix}$$

$$\boldsymbol{C}_{\mathrm{D}}=\begin{bmatrix} c_1\cos^2\theta+c_2\sin^2\theta & -c_2\sin\theta & (c_2-c_1)\sin\theta\cos\theta \\ -c_2\sin\theta & c_2 & -c_2\cos\theta \\ (c_2-c_1)\sin\theta\cos\theta & -c_2\cos\theta & c_2\cos^2\theta+c_1\sin^2\theta \end{bmatrix}$$

$$\boldsymbol{K}_{\mathrm{D}}=\begin{bmatrix} k_1\cos^2\theta+k_2\sin^2\theta & -k_2\sin\theta & (k_2-k_1)\sin\theta\cos\theta \\ -k_2\sin\theta & k_2 & -k_2\cos\theta \\ (k_2-k_1)\sin\theta\cos\theta & -k_2\cos\theta & k_2\cos^2\theta+k_1\sin^2\theta \end{bmatrix}$$

$$\boldsymbol{r}=\begin{pmatrix} x_2 \\ y_1 \\ y_2 \end{pmatrix}$$

$$\boldsymbol{F}=\begin{pmatrix} 0 \\ -F_{\mathrm{ext}} \\ 0 \end{pmatrix} \tag{5}$$

Lastly, considering a sticking condition, the number of DOF is reduced to one, resulting in Eq. (6):

$$\ddot{y}_1=-\frac{1}{m_1}\left[c_2(\dot{y}_1-\dot{x}_2\sin\theta)+k_2(y_1-x_2\sin\theta)+F_{\mathrm{ext}}\right] \tag{6}$$

in which the tangential velocity of the mass m_2 is equal to the belt velocity (v_{belt}).

Before assessing the transient response of the system, its dynamics is evaluated in the following section by CEA.

2.2 Energy balance and contact power flows

In this work, an energy analysis is proposed to investigate the unstable dynamics response of the system and the bi-stable behavior that can be observed for mode coupling instability. To achieve this aim, the flows of acquired, exchanged, and dissipated energy by the system have to be defined, in order to provide an energy-based description of the instability during its onset in linear conditions and at the limit cycle, when nonlinearities modify the energy flows at the contact interface. The energy balance at the contact can be discussed according to Ref. [33]. The total mechanical energy of the elastic body E_{m} is given by the sum of kinetic energy and elastic potential energy, which can be expressed, respectively, as shown in Eq. (7):

$$E_{\mathrm{kin}}=\frac{1}{2}\dot{\boldsymbol{r}}^{\mathrm{T}}\boldsymbol{M}\dot{\boldsymbol{r}},\ \ E_{\mathrm{el}}=\frac{1}{2}\boldsymbol{r}^{\mathrm{T}}\boldsymbol{K}\boldsymbol{r} \tag{7}$$

Variations of total mechanical energy are given by the difference between the work of external forces acting on the body

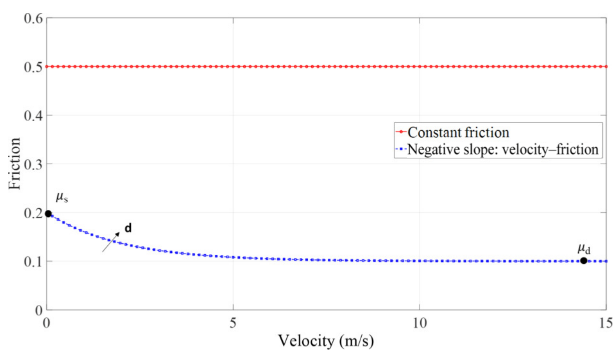

Fig. 2 Constant (red) and exponentially decreasing (blue) friction laws.

and the work of internal non-conservative forces, i.e., the damping terms. Considering the total power exchanged at the contact interface, a part is exchanged between the belt and the mechanical system (P_c), while another part is dissipated directly at the contact (P_{dc}).

The dissipated component is dissipated only during the sliding condition, and is defined as Eq. (8):

$$P_{dc} = T \cdot v_{rel} \tag{8}$$

in which T represents the tangential frictional force at the contact, and v_{rel} is the relative velocity between the mass m_2 and the moving belt.

As concerns the energy exchanged by the belt and the mechanical system, the power is transferred from the belt to the moving mass through the frictional force. Depending on the contact status, the power exchanged between the two bodies assumes two different forms:

In a sticking condition (status = 0), the power exchanged (P_{st}) is defined as the product between T and v_{belt}, equal to the one of the masses m_2, as shown in Eq. (9):

$$P_{st} = T \cdot v_{belt} \tag{9}$$

In sliding condition (status = 1), the power exchanged (P_{sl}) is defined as the product between T and absolute velocity of the elastic body. Being $\dot{x}_2$ the absolute velocity of the mass m_2 on the tangential direction, P_{sl} is defined as Eq. (10):

$$P_{sl} = T \cdot \dot{x}_2 \tag{10}$$

In detachment condition (status = 2), no power is exchanged between the system and the belt, and no energy is dissipated, since no contact is experienced.

Hence, P_c, i.e., the power transferred to the elastic body from the contact, can be considered as the sum of P_{st} and P_{sl}. A positive term indicates a power flowing into the system, while a negative term indicates a power loss from the system, as shown in Eq. (11):

$$P_c = P_{st} + P_{sl} \tag{11}$$

Finally, the power of the external force acting on the mass m_1 can be expressed as Eq. (12):

$$P_{Fex} = F_{ext} \cdot \dot{y}_1 \tag{12}$$

The energy balance of the system can be, then, expressed as Eq. (13):

$$\frac{dE_m}{dt} = P_c - P_{dm} + P_{Fex} \tag{13}$$

in which P_{dm} represents the power dissipated by the system damping c_1 and c_2.

During transient simulations, at each step-time, the values of the different exchanged powers at the contact are calculated. Hence, following the previous equations, integrating the difference $P_c - P_{dm} + P_{Fex}$ in time, it is possible to follow the behavior of mechanical energy exchanged by the system at the contact.

2.3 Model parameters and critical friction coefficients

The set of parameters used for the following analysis is shown in Table 1. The model parameters were chosen so that the system dynamics is characterized by the coupling of the two modes occurring for a realistic value of the friction coefficient, with the additional requirement that the real part of one of the two system eigenvalues became positive after the lock-in of the two modes, thanks to the system damping.

Considering the system in the sliding equilibrium state, complex eigenvalue analysis (CEA) has been carried out by varying the μ_d in order to identify the critical friction coefficient by linear stability analysis. Consequently, the system matrices are the ones considered in Eq. (2), considering the classical Coulomb constant friction coefficient. The method involves calculating the system eigenvalues and their corresponding eigenvectors, which are generally complex-valued functions. The real part of the eigenvalues is used as a parameter to assess the stability of the corresponding mode.

Figure 3(a) shows the natural frequencies (imaginary part of the eigenvalues) of the system, while Fig. 3(b) shows the trend of the real parts of the corresponding eigenvalues, as a function of the friction coefficient. As expected [20], when increasing the friction coefficient, mode coupling occurs, characterized by the coalescence of two modes. The imaginary parts coalesce, while the real parts diverge, and one of them becomes positive, meaning that the corresponding mode is unstable. For the chosen set of parameters, mode coupling occurs for a friction coefficient ($\mu_{coupling}$) equals to 0.22, for which the two modes coalesce with a frequency of 68 Hz.

For friction values lower than the coupling one, the system response is characterized by two modes at different frequencies, with negative real parts of the eigenvalues, resulting in a stable response of the frictional system. At the coupling friction coefficient, the real parts of the eigenvalues diverge. One of the real parts goes toward the positive half-space, and this leads to the identification of a critical value of the friction coefficient (μ_{crit} = 0.23), from which one mode of the system reaches a positive real part of the eigenvalue, which leads to self-excited unstable FIVs. Hence, mode coupling instability can be induced by imposing a friction coefficient that exceeds the critical value μ_{crit}. The linear dynamic analysis of the system predicts that, as the frictional system, when considering an equilibrium position in a sliding state, switches from a stable state to an unstable one, after a bifurcation point.

Table 1 Parameters used in lumped parameters model

Parameter		Value
Mass of the first body	m_1 (kg)	0.53
Mass of the second body	m_2 (kg)	0.045
Damping value of the damper connecting the mass m_1 to the external frame	c_1 (N·s/m)	1
Damping value of the damper connecting the two masses	c_2 (N·s/m)	1
Stiffness of the spring connecting the mass m_1 to the external frame	k_1 (N/m)	100,000
Stiffness of the spring connecting the two masses	k_2 (N/m)	101,000
External normal force	F_{ext} (N)	100
Belt inclination angle	θ (rad)	0.01

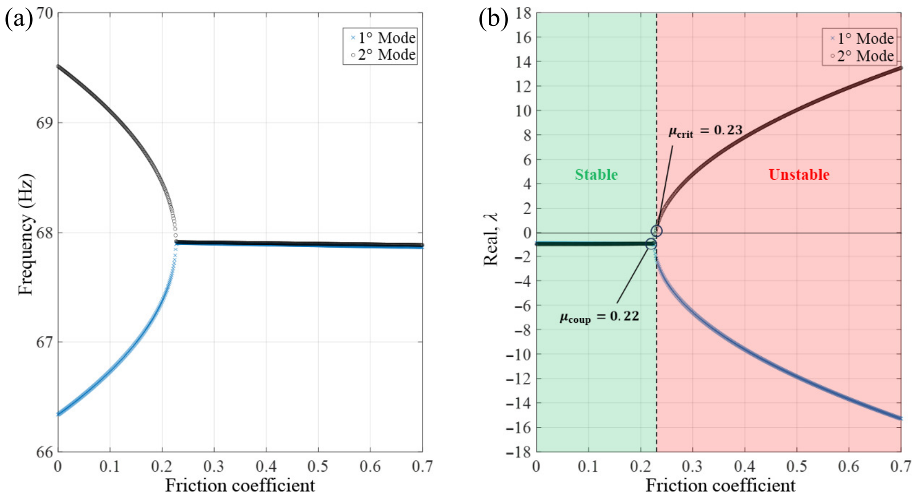

Fig. 3 (a) Natural frequencies and (b) real parts of modes of system as a function of μ, for identification of μ_{crit} for instability occurrence.

3 Transient nonlinear response and energy analysis

Before investigating the bi-stable states of the mode coupling instability from an energy point of view, transient analyses are presented here to simulate the different modal instabilities occurring in the system, as a function of the contact law. In fact, despite providing useful information about the stability of the response in sliding state, the CEA is not sufficient to predict the effective dynamic response of the system under contact nonlinearities, such as contact state or variable friction coefficient. To simulate the effective nonlinear dynamic response, transient simulations have to be performed by the resolution of the equations detailed in Section 2.1. Two test cases have been analyzed, considering either a constant friction coefficient, or a friction-velocity negative slope. In this paragraph, non-linear transient simulations have been conducted to reproduce modal contact instabilities. All the analyses have been performed starting from the sliding equilibrium position, imposing a nil initial velocity for both masses. As concerns the initial position, it has been imposed equal to the static displacement due to the contact forces acting on m_2 during sliding, obtained by the vector product $(\boldsymbol{K})^{-1}\boldsymbol{F}$, where the matrix $\boldsymbol{K}$ and the vector $\boldsymbol{F}$ refer to the one in Eq. (3). From this point, we will refer to x_2 direction as the tangential direction at the contact and, given the small amplitude of the inclination angle θ, to the y_1 direction as the normal direction.

3.1 Mode coupling instability

According to CEA, mode coupling instability can be obtained by setting a constant value of the friction coefficient above the critical friction of 0.23 (Section 2.2). In fact, above such a value, the real part of the eigenvalue correspondent to one of the two coalesced modes assumes a positive value.

A friction law (Fig. 2 (red)) with a constant value of μ set at 0.5 has been used for this simulation, significantly exceeding the critical value for mode coupling occurrence. The v_{belt} has been set to 3 m/s. The obtained normal and tangential accelerations, respectively along the normal and tangential directions, are shown in Fig. 4.

It can be seen how the system response is characterized by an initial exponential increase of the amplitude of vibrations, corresponding to the linear response in full sliding conditions, up to the limit cycle. A magnification during the exponential increase of amplitude of vibrations is shown in Fig. 4(b). A phase shift of almost 90° between normal and tangential accelerations is clearly visible, coherent with the results in literature concerning mode-coupling instability [45, 46]. The exponential increase of oscillations is followed by a limit cycle, due to the onset of contact nonlinearities, which will be discussed in Section 3.3. The spectrogram of the tangential acceleration signal, in Fig. 4(c), shows that during the initiation of the instability (exponential increase), there is only the main harmonic at the coupling frequency of approximately 68 Hz, whereas when nonlinearities arise, referring to both sticking and detachment, super-harmonics are generated with frequencies that are multiples of the fundamental one, originated by the nonlinearities occurring during the limit cycle. Furthermore, the onset of nonlinearities causes a slight decrease in the frequency of the fundamental harmonic, due to a softening of the system when detachments occur.

3.2 Negative slope instability

In this section, non-linear transient simulations have been performed with parameters set to reproduce the system dynamic response under a negative friction-velocity slope characteristic. The μ_s and μ_d have been set respectively at 0.2 and 0.1 and an exponential decreasing law compared to relative velocity has been imposed, according to Eq. (1) with decaying coefficient equal to 0.5. It must be noted that both values have been set under μ_{crit} (0.23), in order to avoid mode coupling occurrence.

The analysis has been performed imposing v_{belt} of 0.5 m/s, i.e., a value falling within the range where the friction coefficient results in being strongly affected by the sliding velocity, decreasing when the velocity increases. In this case, the system response, as shown in Fig. 5(a), exhibits an unstable behavior, characterized by an exponential increase of amplitude of vibrations, up to a limit cycle. The negative friction-velocity slope is enough to result in an unstable system response. Effectively, a threshold value exists for the rate at which friction the coefficient decreases compared to an increase in relative velocity, leading to an apparent negative modal damping and consequently to the instability. Focusing on the instability onset phase, the zoom of normal and tangential accelerations in Fig. 5(b) shows the in-phase behavior of the two signals, which is consistent with results in Refs. [45, 46]. In this case, the spectrogram of the tangential acceleration in Fig. 5(c) shows that even at limit cycle only one harmonic is detected at the coupling frequency of 68 Hz.

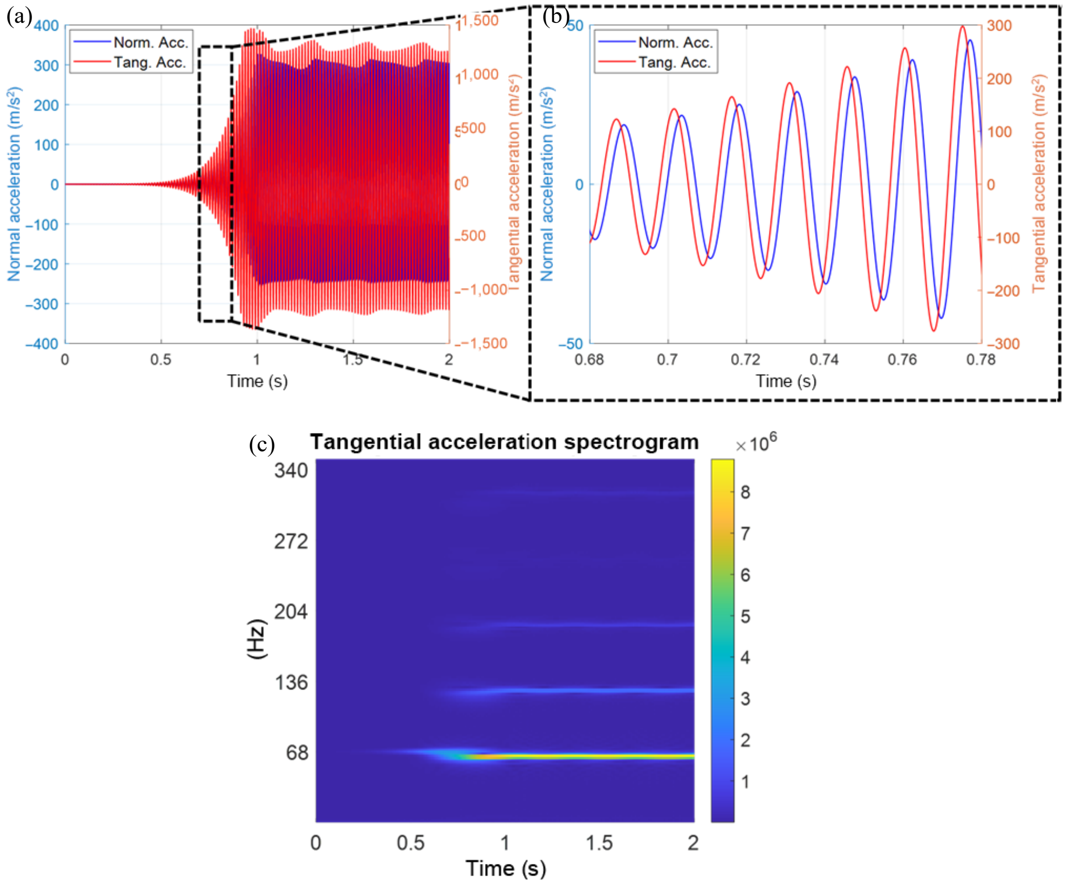

Fig. 4 (a) Accelerations along x_2 direction (red) and y_1 direction (blue) obtained for a simulation with $\mu_s = \mu_d = 0.5$ and v_{belt} of 3 m/s. (b) Zoom on exponential increase of oscillation to observe phase shift of acceleration dynamics. (c) Tangential acceleration spectrogram.

In this case, the only source of nonlinearity is the sticking phase, which alone is not sufficient to excite the system at frequencies higher than the fundamental one. In contrast, in mode coupling instability, the alternation between sticking and detachment introduces discontinuities that lead to the generation of higher-order harmonics.

3.3 Coexistence of negative slope and mode coupling instability

In this section, the friction law has been set to investigate the possible co-existence of mode coupling and negative slope instabilities. At this aim, an exponential friction law with a static coefficient μ_s of 0.6 and a dynamic one μ_d of 0.5 has been used. This law maintains the same trend used for the negative slope instability, discussed in Section 3.2, but with different values, which exceed the critical friction coefficient, inducing mode coupling and negative slope instability at the same time. The v_{belt} has been imposed constant and equal to 0.5 m/s to ensure a sufficient negative friction-velocity slope to induce the instability. The results of the simulation are reported in Fig. 6(a), where the obtained tangential acceleration in the coexistence scenario is compared with that from the two individual cases, each simulated at the same imposed velocity of 0.5 m/s.

It can be noted that the system concerned with both negative slope and mode coupling instability behaves similarly to the other cases, but a faster exponential increase of oscillation is observed. This observation can be explained by the overlapping of the effects of mode coupling and negative slope in increasing the real part of the unstable eigenvalue, which drives the exponential increase of vibration amplitude. Afterwards, when the system reaches the steady state, the maximum oscillation at the limit cycle is close to, and slightly higher, than the one obtained by mode coupling instability alone. Moreover, the phase shift in the accelerations is also noted (Fig. 6(b)), due to the presence of the two coalesced modes that lead to the phase shift between the normal and tangential DOF. Lastly, it can be observed how, for this set of parameters, the system behavior presents three different phases. After the initial exponential increase in vibration amplitude, a progressive linear growth is observed before reaching the limit cycle. In Fig. 7, an energy analysis is performed at the three different phases highlighted in Fig. 6(a), focusing on the mechanical power, expressed as the difference between the power entering the system both from the contact and due to the external forces and the one dissipated by the system damping. Figure 7 highlights how the change in system behavior depends on the onset of nonlinear phenomena. Specifically, the transition from exponential to linear growth is due to the appearance of sticking periodic phenomena that arise when the mass m_2 is expected to accumulate the highest amount of power from its relative motion with the belt, as shown in Fig. 7(a). This phenomenon, non-observable in Fig. 4(a), can be justified by the reduction of the imposed v_{belt} with respect to the one used for the characterization of mode coupling instability, which makes it easier to reach the sticking condition. During the linear growth phase, the system gains energy at each cycle and uses it to increase its oscillation amplitude. Consequently, the cumulated power per cycle tends to increase as well. However, Fig. 7(b) shows that the sticking phase duration also increases over time. These two effects balance each

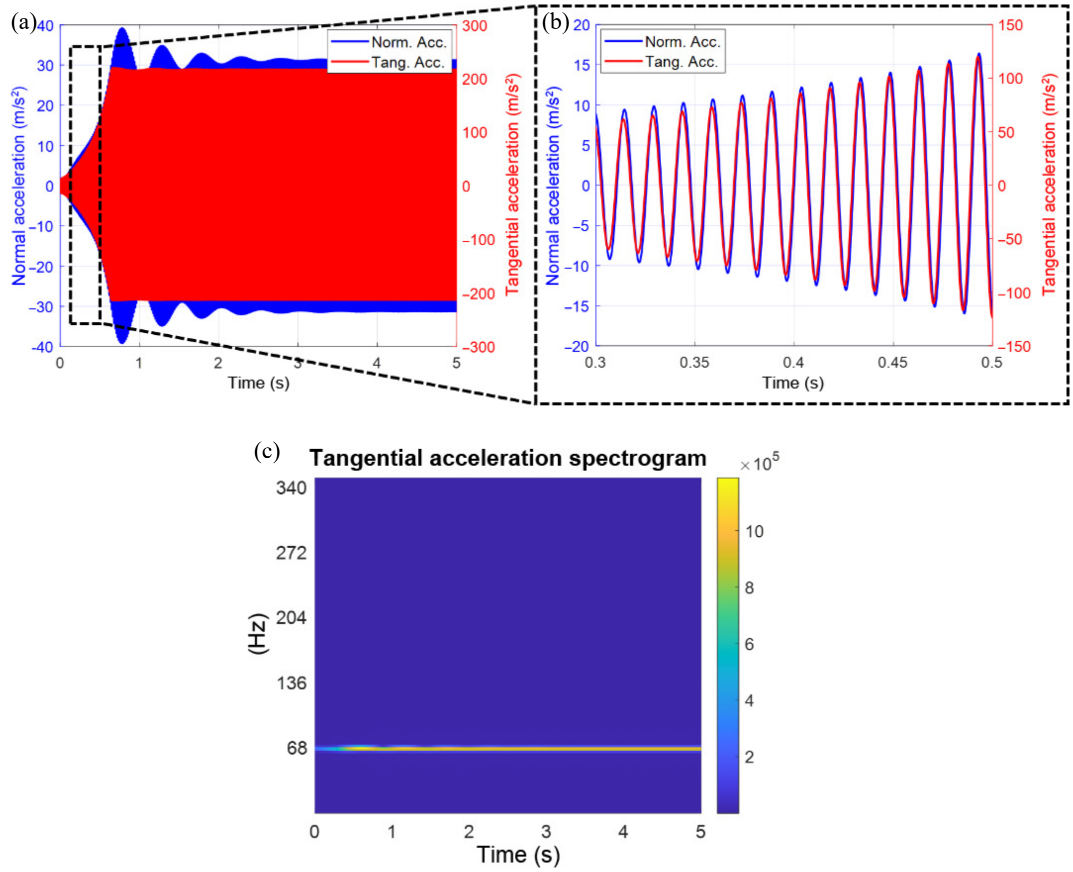

Fig. 5 (a) Accelerations along x_2 direction (red) and y_1 direction (blue) for an exponentially decreasing friction coefficient ($\mu_s = 0.2$, $\mu_d = 0.1$, and $d = 0.5$), and for a constant velocity belt of 0.5 m/s. (b) Zoom on exponential increase of oscillation to observe in phase behavior of acceleration dynamics. (c) Tangential acceleration spectrogram.

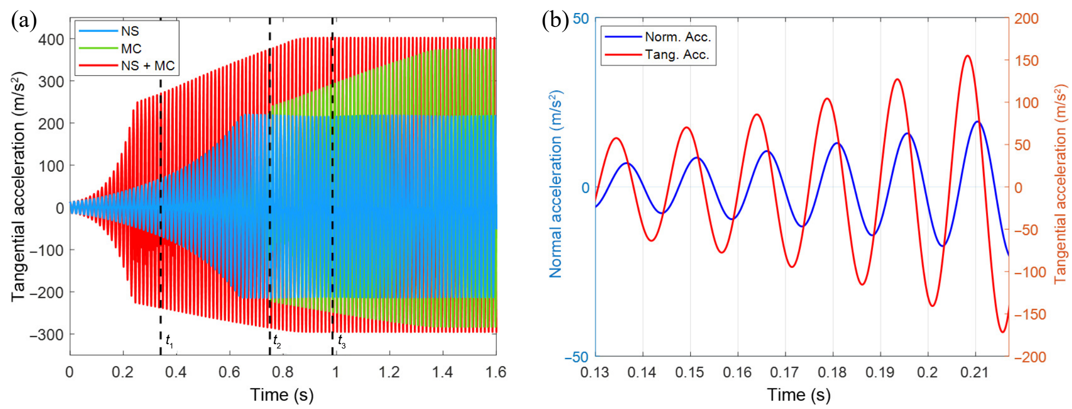

Fig. 6 (a) Tangential accelerations of unstable responses due to negative slope (blue), mode coupling (green), and their coexistence (red). (b) Zoom on exponential increase of oscillation during mode coupling and negative slope coexistence to evidence phase shift between normal and tangential oscillations.

other, making the increase in oscillation amplitude linear, meaning the energy accumulated per cycle by the system remains constant until the limit cycle is reached. At this point, the nonlinear phenomena further change, with the appearance of detachment phases, and thus the power flows are also modified, preventing the system from accumulating energy cycle by cycle to further increase its oscillation amplitude (Fig. 7(c)).

4 Mode coupling bi-stable states and energy analysis

In this section, the bi-stable characteristic of the mode coupling instability, i.e., the possibility to detect a bi-stable region as a function of a system key parameter (here the friction coefficient) and of an external perturbation, is investigated. Specifically, an impulsive perturbation is introduced to verify the possibility of triggering the mode coupling instability when the system is in the stable region previously identified by the CEA (i.e., the imposed friction coefficient is lower than the critical one), switching the system state from stable sliding to mode coupling oscillations. Additionally, the role of contact nonlinearities on the energy flows at the contact interface is analyzed, providing an energetic explanation for the observed bi-stable behavior.

4.1 Bi-stable region detection

The initial model parameters are set to obtain a configuration

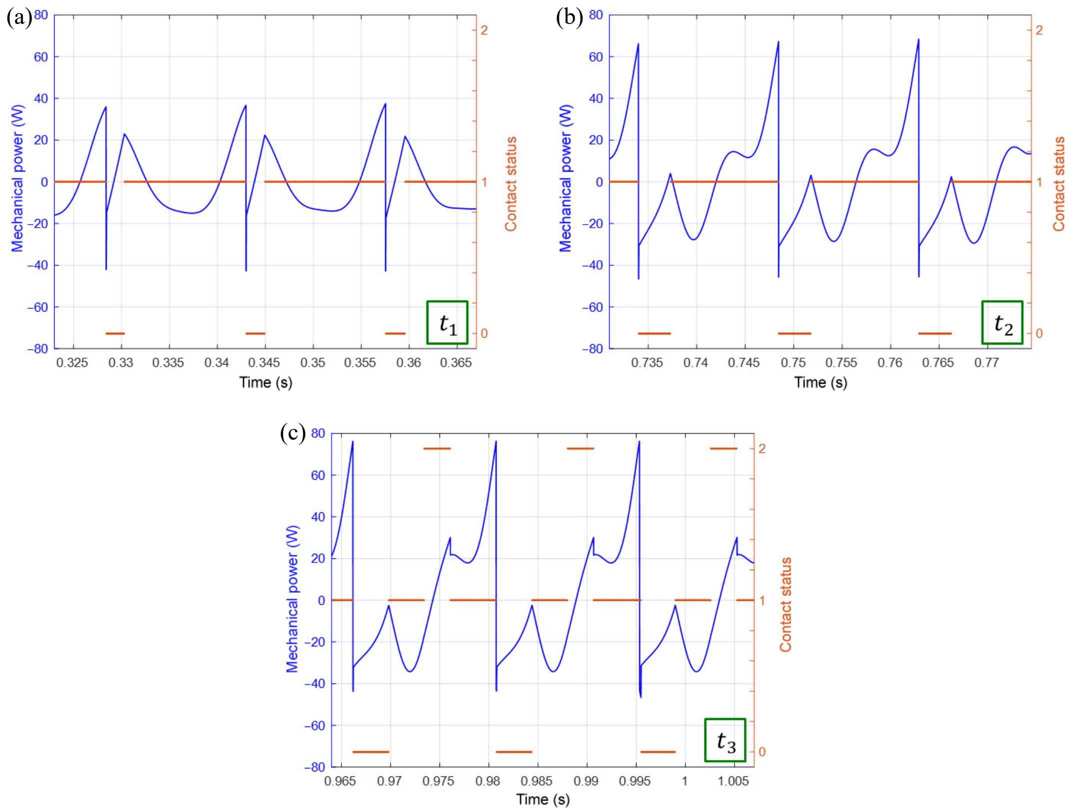

Fig. 7 Mechanical power (blue) accumulated by mass m_2 and contact status (red) during coexistence of mode coupling and negative slope instability, analyzed during initial (t_1) and final (t_2) phases of linear increase in vibrations amplitude observed in Fig. 6(a) and during limit cycle (t_3).

falling in the stable region identified by the CEA in Section 2.2. Then, a perturbation is applied to the system. The perturbation is represented by an impulsive external excitation, obtained by increasing the external force acting on m_1 for a time interval of 0.1 s. The value of the impulsive excitation is defined as Eq. (14):

$$F_{\mathrm{P}} = p \cdot F_0 \tag{14}$$

in which F_0 represents the initial normal force value and F_{P} the value of the perturbation, defining p as the perturbation coefficient. The typical trend of the force presents a step shape, as shown in Fig. 8.

All the simulations presented in this section have been executed imposing an initial normal force F_0 of 100 N, with a constant friction coefficient chosen below its critical value (i.e., stable region expected by the linear CEA analysis). The perturbation on the system has been given after 40 s of simulation, to ensure the system is in the sliding equilibrium position.

The critical friction coefficient for the investigated configuration is 0.23, and the system is predicted to be stable under such values. Transient simulations, without external impulsive excitation, confirm a stable continuous sliding of the system, without relevant vibrations. If the external perturbation excites the system, during the impulsive excitation, a further energy is introduced into the system. Depending on the magnitude of the perturbation, the system state after the perturbation can converge toward two different stable states: either the stable sliding state (Fig. 8) or the limit cycle stable state, characteristic of mode-coupling instability (Fig. 9 (blue)). Specifically, a threshold value for p has been found, above which the onset of the mode coupling instability up to the limit cycle is observed. For p under the critical one, instead, the system response presents an initial increase of amplitude of vibrations due

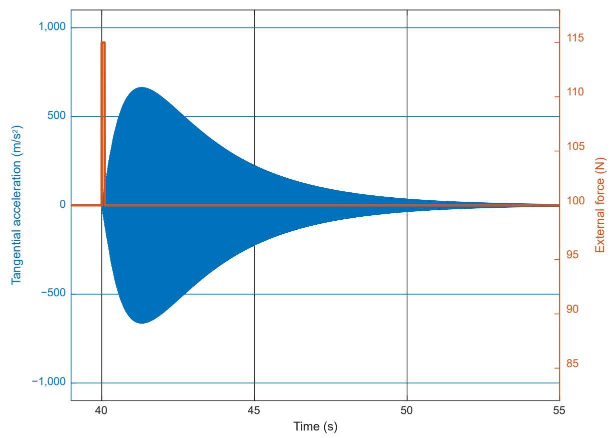

Fig. 8 Typical trend of impulsive perturbation of normal external force (red) and resulting oscillatory response of system (blue).

to the transient response at the perturbation, which is then damped by the system.

Figure 9 presents an example of the performed parametric analysis, in which the constant friction coefficient is set to 0.227. In this case, the tangential acceleration of the mass m_2 is analyzed for two different values of p, one (blue curve) beyond the critical value and the other (yellow curve) below it. After the perturbation, the system shows respectively either mode-coupling leading to a second stable state at the limit cycle or a stable sliding state.

This result shows how the system, under the same boundary conditions and system parameters, can either respond with stable sliding or mode coupling vibrations, depending on the applied perturbation, highlighting the bi-stable nature of the system under mode coupling instability.

The critical value of the external excitation has been identified by a parametrical analysis for different values of the imposed friction coefficient. The results are presented in Fig. 10.

It can be observed that it is possible to induce mode coupling instability even far from μ_{crit} determined for the linear system (Section 2.2), with values of μ even lower than $\mu_{coupling}$, for which the linear CEA does not predict the coalescence of the modes. However, as the friction coefficient is reduced, the value of the necessary perturbation to induce mode-coupling instability increases. As expected, over the critical friction coefficient there is no need of external perturbation (p_{crit} = 1) to trigger the mode coupling.

4.2 Energy analysis of the bi-stable region

In order to understand the underlying physical phenomena at the origin of the bi-stable system response which allows for switching from a one state to another, an energy analysis during the onset of the instability has been performed. The energy flows at the contact, the energy dissipated in the damping elements, and the potential and kinetic energy cumulated by the system are calculated in time and analysed. The contact status has been followed as well, in order to investigate the role of the contact nonlinearities on the triggering of the mode-coupling instability, when the linear system is predicted to be stable by CEA.

The mechanical energy of the system (E_m), during the instability onset, is cumulated cycle after cycle and increases exponentially, in agreement with the exponential increase of the system vibrations. An example is shown in Fig. 11(a), in which the trend of the mechanical energy of the system discussed in Section 3.1 is presented.

In Fig. 11(b), the same analysis is focused on the limit cycle phase. It can be noted how, during this phase, the mean energy content is constant, meaning that an energy equilibrium is reached thanks to the onset of the contact nonlinearities, preventing the system to accumulate additional energy to increase its amplitude of vibration, which shows a self-similar behavior over time, as depicted in Fig. 4(a).

For the mode-coupling case, when the instability arises, the exchanged power at contact P_c, integrated over a cycle, shifts toward positive values. Therefore, an increase of the mechanical energy of the system is observed, as shown in Fig. 12, with this phase lasting until the establishment of the limit cycle, associated with a mechanical energy content oscillating around a constant mean value. In Fig. 12, the total mechanical energy is calculated for both a value of p lower than the critical one (yellow) and a value of p over the critical one (blue).

A more in-depth analysis of the energy balance is performed, focusing on the single cycles of vibrations, to understand the differences in the energy flows that lead to the different responses (Fig. 13).

When the perturbation amplitude is higher than the critical one, the excited system starts to accumulate energy at each cycle and to increase its amplitude of vibrations. Figure 13 focuses on

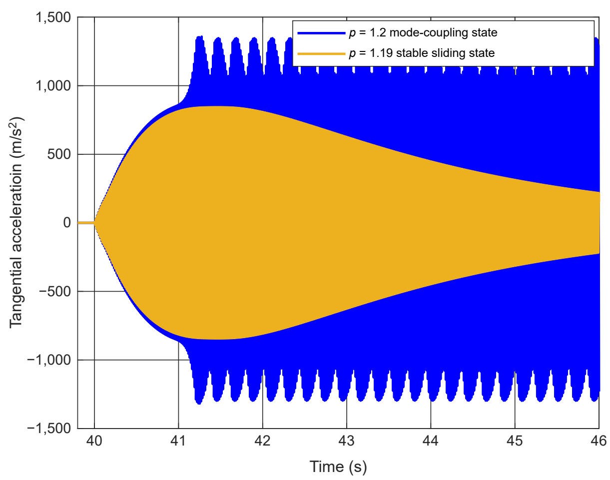

Fig. 9 Dynamic response in tangential direction due to force perturbation for p = 1.2 (blue) and p = 1.19 (yellow) for a system with constant μ_d of 0.227, constant v_{belt} of 3 m/s, and initial external force of $F_0 = 100$ N.

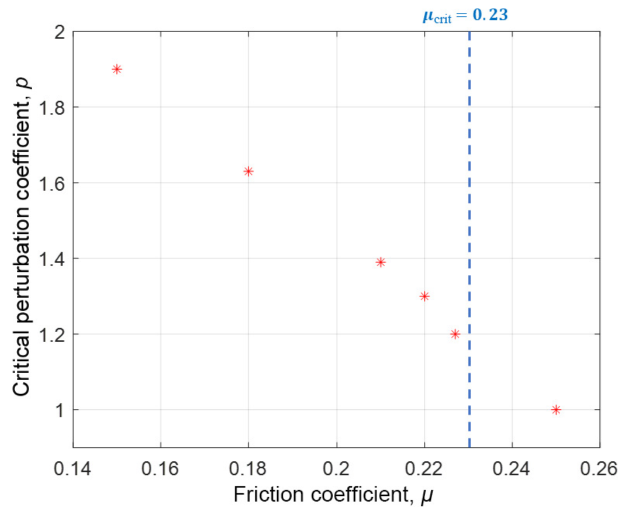

Fig. 10 Values of necessary perturbation coefficient to induce mode coupling instability for different μ_d, with v_{belt} set to 3 m/s and initial external force at 100 N.

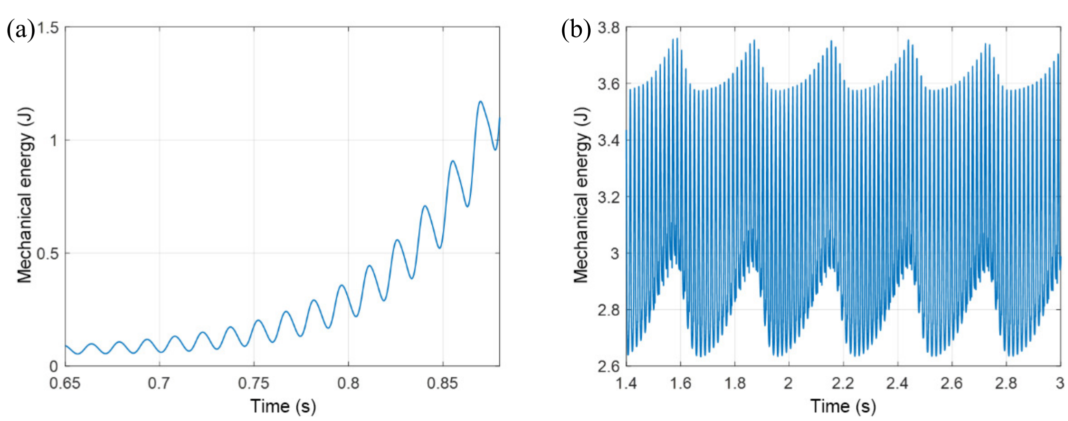

Fig. 11 Mechanical energy cumulated during mode coupling: (a) instability onset and (b) limit cycle.

two cycles of vibrations during the exponential growth phase. It can be seen that, during this phase, the system oscillations due to the impulsive excitations are large enough to make detachment events occur. Moreover, the zoom presented in Fig. 13 evidences that detachment happens when the mass moves from the maximum x_2 position toward the equilibrium one, with its tangential velocity in the opposite direction compared to the belt one. During this phase, the system should lose energy at the contact, because of the opposite sign between its velocity at the contact and the tangential contact force (negative power). Nevertheless, because of the detachment occurring during this phase, no power is exchanged, as shown in Fig. 13 (green curve), and there is an excess of undissipated energy, compared to the same cycle when detachment does not occur. Therefore, the system accumulates energy and further increases its amplitude of vibrations, consequently increasing also the duration of the detachment phase during each cycle. The self-feeding mechanism, at the origin of mode coupling instabilities in the nonlinear system, is therefore allowed by the occurrence of the contact nonlinearities, triggered by an enough large external perturbation. On the contrary, when the external perturbation amplitude is lower than the critical value, the detachment phase is either absent or too short, and the energy is dissipated at the contact during the transient response of the system, which returns to its stable sliding state.

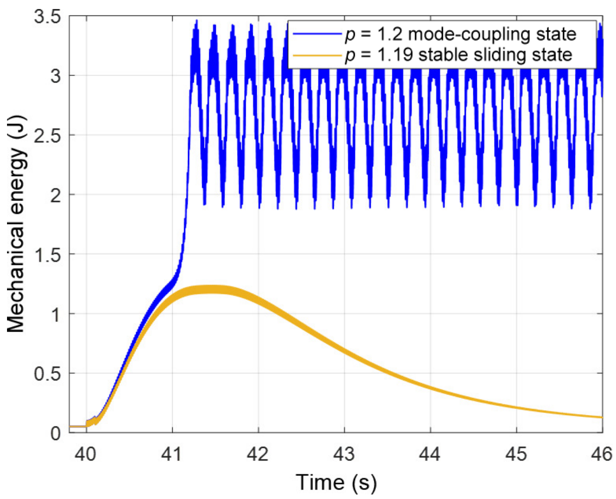

Fig. 12 Total mechanical energy of system calculated for an external force perturbation with $p = 1.2$ (blue) and $p = 1.19$ (yellow).

Referring to the same comparison made in Fig. 12, it can be observed that for p = 1.19 the detachment events that arise are shorter compared to the ones for p = 1.2, as it can be observed in the magnifications in Fig. 14. Therefore, the system is able to dissipate a higher amount of energy through the sliding contact, resulting in the return to a stable sliding state. Hence, not sufficiently large perturbations result in mechanical oscillations that do not lead to the instability onset.

It is worth reminding that, for the chosen friction coefficient and system parameters, the CEA of the linearized system predicts stable eigenvalues, because detachment nonlinearities are not taken into account.

These results highlight how, when considering the nonlinear dynamics of a frictional system, the effect of the contact nonlinearities on the mechanical energy flows can explain the switching between two stable states of the system response.

4.3 Effect of belt velocity

Having highlighted how the possibility to switch from a stable state to the other depends on the energy balance per cycle of oscillation, affected by contact nonlinearities, it is interesting to investigate the effect of the amount of external power provided by the contact. Then, a parametrical analysis has been conducted varying the v_{belt}, to investigate the influence of this parameter on the bi-stable behavior of the system. The friction coefficient set for this analysis is $\mu = 0.227$, constant and close to the unstable region. The results are presented in Table 2.

It can be observed that, as the v_{belt} increases, the perturbation necessary to trigger the mode coupling instability, and switch from the stable sliding state to the mode-coupling limit cycle, also increases, up to a given value of the v_{belt}, specifically 3 m/s, after which it remains constant.

Figure 15(a) shows the dynamic behavior of the system, with

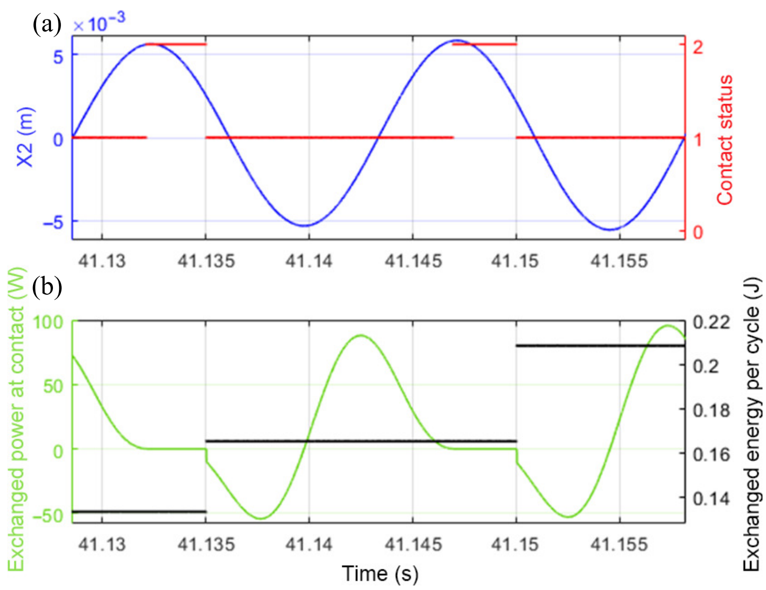

Fig. 13 Magnification on two cycles during exponential increase of amplitude of vibrations, due to mode coupling triggering through impulsive variation of external force: (top) tangential displacement (blue) and contact status (red); (bottom) exchanged power at contact (green) and exchanged energy per cycle at contact (black) ($\mu_s = \mu_d = 0.227$, $v_{\mathrm{belt}} = 3$ m/s, and $p = 1.2$).

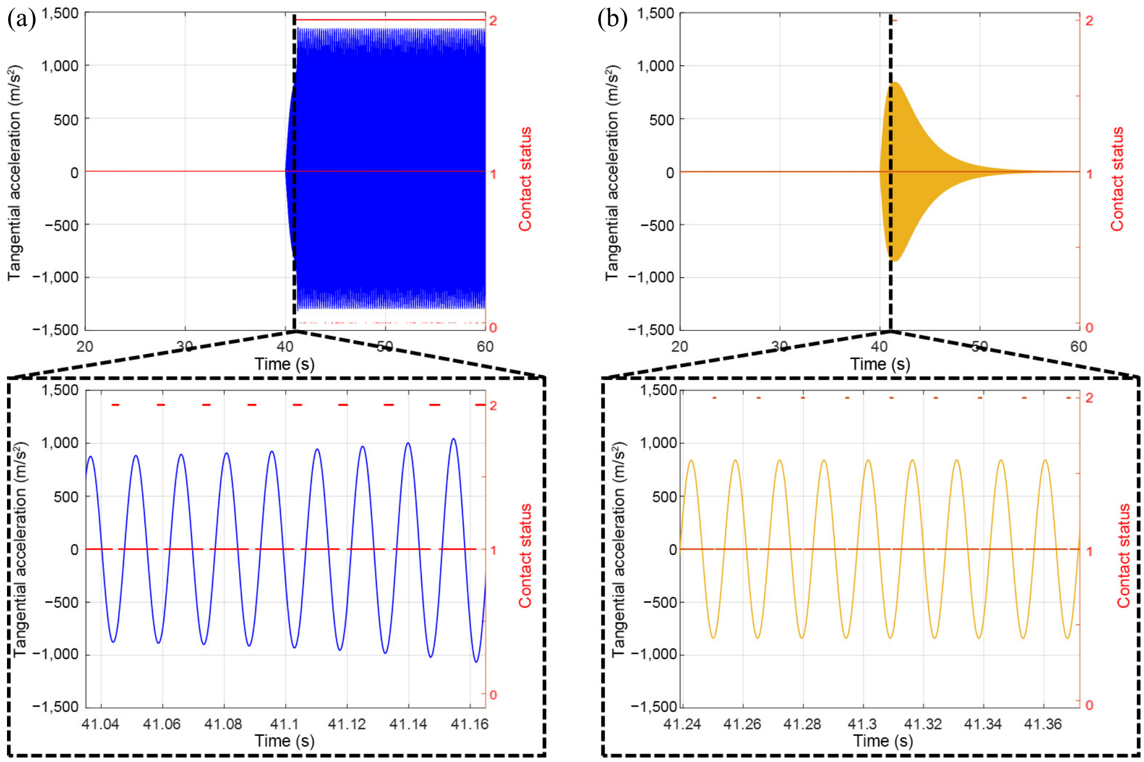

Fig. 14 Role of contact nonlinearities on system behavior for (a) $p = 1.2$ and (b) $p = 1.19$.

v_{belt} of 1 m/s and p of 1.6, above the critical value for the occurrence of instability for this set of parameters. It can be observed that the initial increase of amplitude of oscillation, due to the effects of the perturbation, is interrupted by the rise of sticking events, which occur earlier than detachment conditions. During this phase, the amplitude of vibrations increases almost linearly with the time. A more in-depth analysis can be performed looking at the magnification in Fig. 15(b), in which a couple of cycles is analyzed by an energy approach. It can be observed that the system undergoes sticking conditions as it increases its tangential velocity, preventing it from exceeding the v_{belt} and inverting the sign of the relative speed. Such an inversion would lead to a reversal of the tangential friction force, while keeping the velocity of the system unchanged in sign. Consequently, the power exchanged at the contact, P_c, would switch from entering the system to being dissipated. Therefore, the sticking condition prevents this energy dissipation, leading instead to further energy accumulation at each cycle. The black curve in the bottom graph of Fig. 15(b) confirms that the energy accumulated at the contact during each cycle is positive, resulting in a continuous increase of total mechanical energy in the system. This behavior persists until detachment events occur, ultimately leading to instability.

Figure 16(a) shows the results of the same analysis performed with an imposed v_{belt} of 1.5 m/s. Since a friction law independent of the v_{belt} has been imposed, the system response remains unchanged until nonlinearities emerge. Since a higher velocity is needed to match that of the belt, the sticking condition occurs later in this system. However, as the oscillation frequency remains the same between the two cases, the time spent at higher velocities is shorter, leading to a shorter sticking phase. When the sticking phase becomes too brief, it fails to supply sufficient additional energy to compensate for the energy dissipated in each cycle. Consequently, the system is unable to reach the detachment condition, preventing the mode coupling instability from onset. Therefore, a stronger perturbation is required to enhance the system dynamics and extend the duration of the sticking phase, allowing instability to develop. This is evident looking at the black lines in the bottom figure of Fig. 16(b), which shows that the total mechanical energy of the system at each cycle is negative, resulting in the damping of its oscillation up to a point at which no more sticking condition is reached, and the system dynamics returns to its equilibrium condition.

Table 2 Values of necessary perturbation coefficient to trigger mode coupling instability for different v_{belt}, with μ set to 0.227 with initial external force of 100 N

v (m/s)	Critical p
0.5	1.06
1	1.11
1.5	1.17
3	1.20
5	1.20
10	1.20
100	1.20

Starting from v_{belt} of 3 m/s, no more sticking condition is experienced and instability is generated only due to detachment events, as discussed in Section 4.2.

Moreover Fig. 17, which shows the phase plane displacement-velocity along the x_2 direction, highlights how, starting from this point, although the necessary perturbation to induce the instability does not change, increasing the v_{belt} the system acquires more energy from the contact and further increases its amplitude of vibrations at the limit cycle. Starting from a v_{belt} equal to 10 m/s, however, the system demonstrated a threshold in the amplitude of the limit cycle, behaving consistently regardless of the imposed belt speed.

In order to physically explain this phenomenon, Fig. 18(a)

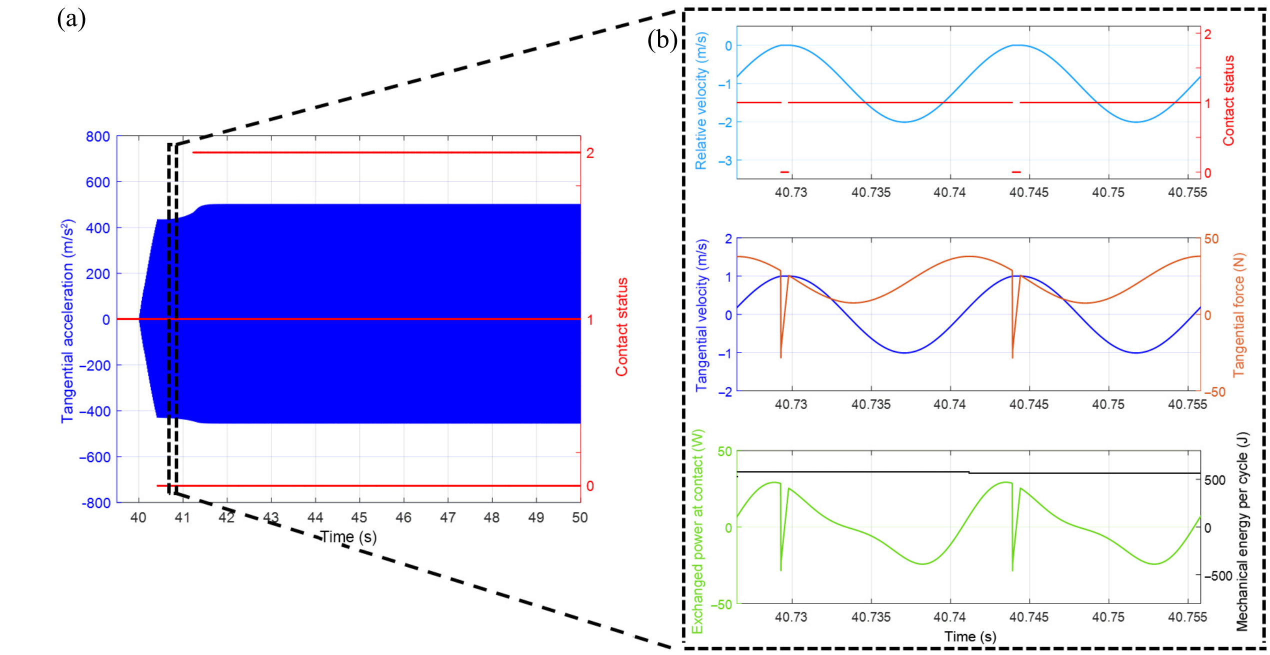

Fig. 15 (a) Tangential acceleration and contact status of a system characterized by constant μ of 0.227, v_{belt} of 1 m/s, and an external force of 100 N, subjected to a perturbation of $p = 1.16$. (b) Magnification on two cycles of the response for energetical considerations.

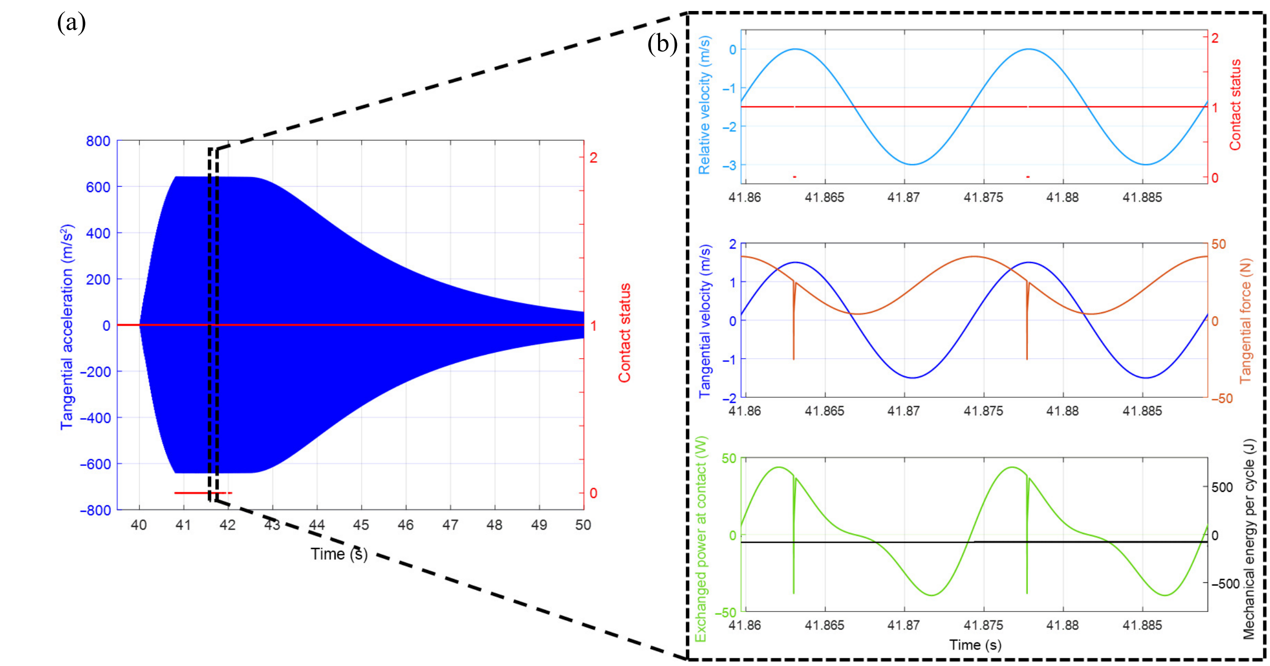

Fig. 16 (a) Tangential acceleration and contact status of a system characterized by constant μ of 0.227, v_{belt} of 1.5 m/s, and an external force of 100 N, subjected to a perturbation of $p = 1.16$. (b) Zoom on two cycles of response for energetical considerations.

shows the dynamic response of the system to a perturbation of $p = 1.2$ for v_{belt} of 3 m/s and 10 m/s. It can be observed that the response of the system is the same during the instability onset, regardless of the imposed v_{belt}. This is justified by the fact that the imposed friction law does not depend on the v_{belt}. As a result, the frictional motion depends only on the system dynamics, which results in remaining consistent in the different scenarios up to the occurrence of nonlinearities.

Conversely, at limit cycle, differences in vibration amplitude are evident, with the 3 m/s scenario showing lower vibration amplitude. To better understand this behavior, energy considerations must be discussed.

Figure 18(b) presents the values of relative and absolute tangential velocity and T for the case with an imposed v_{belt} of 3 m/s. It can be observed that, during the oscillations at the limit cycle, a change in sign of the relative velocity is experienced, resulting in an opposite direction of the frictional force, while keeping the absolute tangential velocity consistent in sign. This causes a change in the sign of the exchanged power at the contact, which is dissipated by the system rather than cumulated. Consequently, the energy stored by the system at each cycle is lower, resulting in a reduced amplitude of vibrations.

Figure 18(c) shows that, at a v_{belt} equal to 10 m/s, the change in sign of relative velocity is no more experienced, hence preventing the system from dissipating the energy at the contact during the movement towards positive x_2. As a result, the system behavior

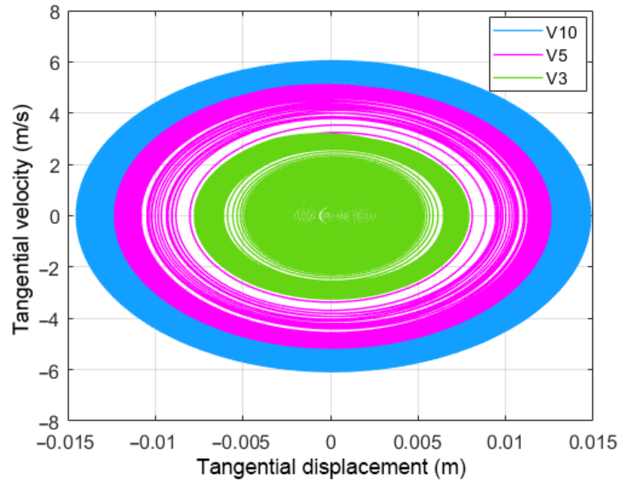

Fig. 17 Phase planes plot of tangential displacement representing unstable dynamic response of system due to external perturbation for different v_{belt} of 3 m/s (green), 5 m/s (purple), and 10 m/s (blue).

reaches a saturation in response from an energetic point of view and remains consistent even further increasing the v_{belt}, indicating that the system cannot store additional energy.

5 Conclusions

In this work, an energy analysis on a lumped numerical model has been developed to investigate the phenomena underlying the bi-stable behavior observable on frictional systems, where different dynamic states (continuous stable sliding or mode-coupling vibrations) can be obtained for the same operating conditions, triggered by an external perturbation. With this aim, contact nonlinearities have been implemented in the model for nonlinear transient analyses, introducing the possibility to switch between three different contact status, from sliding conditions to sticking or detachment ones.

The presence of a bi-stable behavior of the system has been then pointed out, highlighting how an external perturbation applied on a system operating in the stable region of the linearized system (determined by CEA), is capable to trigger a mode coupling instability. With respect to previous works in literature, an energy approach has been introduced to explain the underlying physics leading to the switch from a stable-state to the other one. In detail, a sufficiently high perturbation is able to furnish the system enough energy to activate the contact nonlinearities, which modify the energy flows at the contact. The energy balance at the contact has been then performed, identifying the presence of a

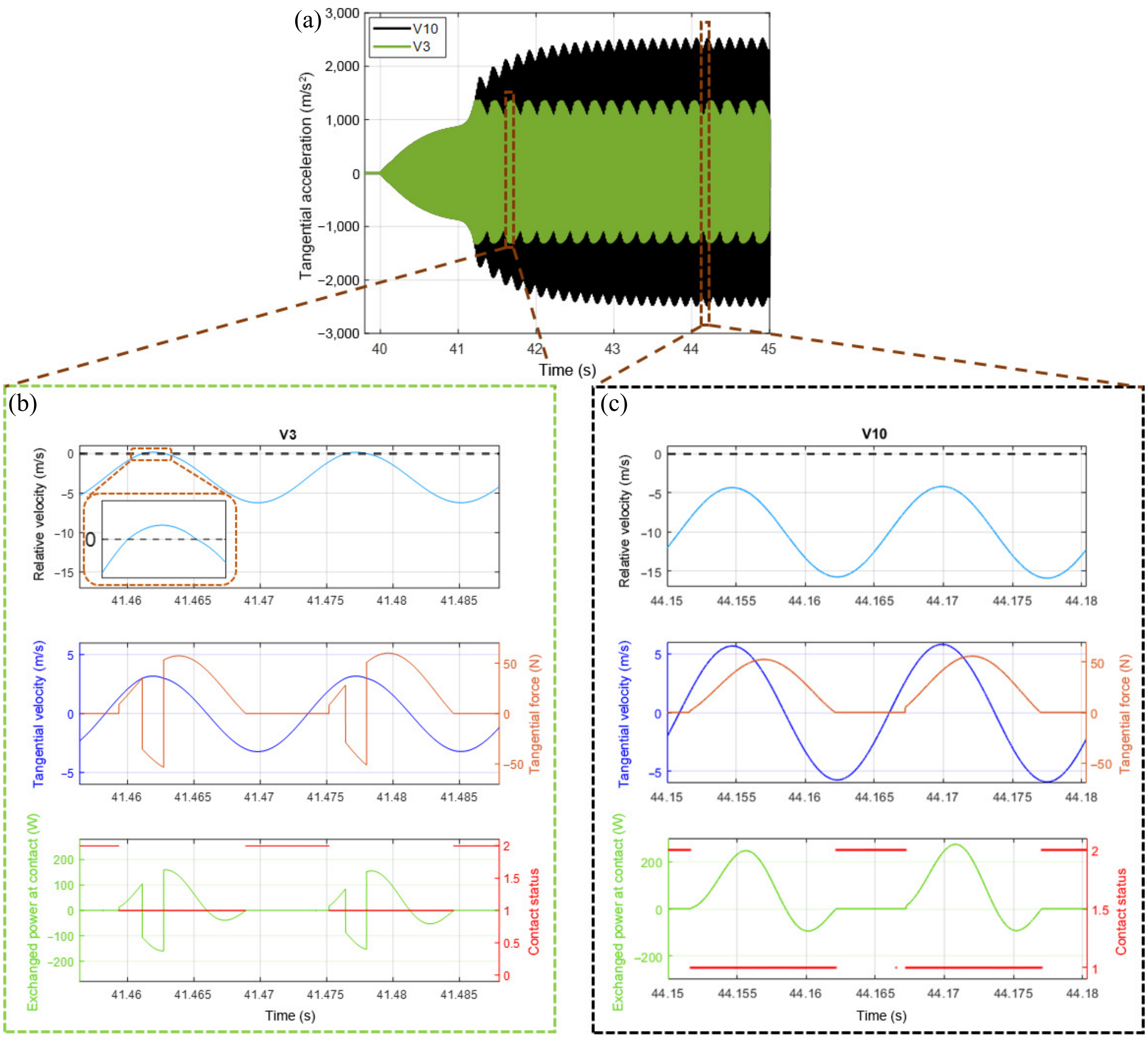

Fig. 18 (a) System response for a perturbation p = 1.2, for v_{belt} of 3 m/s and 10 m/s; zoom on two cycles at limit cycle to understand energy flows for (b) 3 m/s and (c) 10 m/s scenarios.

threshold value for the perturbation to induce a self-exciting non-linear mechanism. The key role of the contact nonlinearities in modulating the energy flows at the contact has been discussed, highlighting the possibility of obtaining different types of dynamic responses depending on the involved non-linear contributions to the energy balance for cycle of oscillation. It should be noted that, focusing on the mode-coupling mechanical instability, only mechanical energy flows have been investigated, simulating the macroscopic nonlinear dynamics of the system, but neglecting microscopic interface phenomena, which can largely affect the overall system response. In the model, the interface interactions are reduced to the sliding/sticking/detachment contact status, and the average frictional resistance is modeled through a friction coefficient. Although the analysis is conducted on a simplified lumped model, allowing for the identification of the different energy contributions, the identified mechanisms may partially explain the fugitive nature of mode coupling instability and the variability observed in its occurrence on real frictional systems.

Declaration of competing interest

The authors have no competing interests to declare that are relevant to the contents of this article.

References

[1] Akay A. Acoustics of friction. *J Acoust Soc Am* **111**(4): 1525–1548 (2002)

[2] Zhang Q X, Ouyang H J, Liu H, Mo J L, Tang B, Zhu S, Jin W W. A lumped-parameter model for stick–slip vibration in train brake systems considering hexagonal friction block sizes. *Mech Syst Signal Pr* **228**: 112486 (2025)

[3] Stender M, Di Bartolomeo M, Massi F, Hoffmann N. Revealing transitions in friction-excited vibrations by nonlinear time-series analysis. *Nonlinear Dynam* **98**(4): 2613–2630 (2019)

[4] Ibrahim R A. Friction-induced vibration, chatter, squeal, and chaos: Part II: Dynamics and modeling. *Appl Mech Rev* **47**(7): 227–253 (1994)

[5] Papangelo A, Putignano C, Hoffmann N. Critical thresholds for mode-coupling instability in viscoelastic sliding contacts. *Nonlinear Dynam* **104**(4): 2995–3011 (2021)

[6] Ghezzi I, Tonazzi D, Rovere M, Le Coeur C, Berthier Y, Massi F. Frictional behavior of a greased contact under low sliding velocity condition. *Tribol Int* **155**: 106788 (2021)

[7] Wang X F, Mo J L, Ouyang H J, Xiang Z Y, Chen W, Zhou Z R. Simultaneous energy harvesting and tribological property improvement. *Friction* **9**(5): 1275–1291 (2021)

[8] Chen F, Ouyang H J, Wang X C. A new mechanism for friction-induced vibration and noise. *Friction* **11**(2): 302–315 (2023)

[9] Cai Z B, Chen Z Q, Sun Y, Jin J Y, Peng J F, Zhu M H. Development of a novel cycling impact–sliding wear rig to investigate the complex friction motion. *Friction* **7**(1): 32–43 (2019)

[10] Chen W, Zhang Q X, Mo J L, He Z C, Wang X C, Zhu S, Zhao C G. Experimental and numerical investigation on the brake interfacial tribology behavior of high-speed train under long-ramp braking conditions. *Friction* **14**(5): 9441130 (2026)

[11] Wang Z W, Mo J L, Zhao C G, Wang Q, Wang K Y. Dynamic modeling and brake stick-slip vibration analysis of a vehicle-track system with disc-pad nonlinear frictions. *Tribol Int* **202**: 110317 (2025)

[12] Thévenot M, Brunel J F, Brunel F, Bigerelle M, Stender M, Hoffmann N, Dufrénoy P. *In situ* operando indicator of dry friction squeal. *Lubricants* **12**(12): 435 (2024)

[13] Rhee S K, Jacko M G, Tsang P H S. The role of friction film in friction, wear and noise of automotive brakes. *Wear* **146**(1): 89–97 (1991)

[14] Eriksson M, Lord J, Jacobson S. Wear and contact conditions of brake pads: Dynamical *in situ* studies of pad on glass. *Wear* **249**(3–4): 272–278 (2001)

[15] Kinkaid N M, O'Reilly O M, Papadopoulos P. Automotive disc brake squeal. *J Sound Vib* **267**(1): 105–166 (2003)

[16] Dieterich J H. Time-dependent friction and the mechanics of stick-slip. *Pure Appl Geophys* **116**(4): 790–806 (1978)

[17] Ruina A. Slip instability and state variable friction laws. *J Geophys Res–Sol Ea* **88**(B12): 10359–10370 (1983)

[18] Shin K, Brennan M J, Oh J E, Harris C J. Analysis of disc brake noise using a two-degree-of-freedom model. *J Sound Vib* **254**(5): 837–848 (2002)

[19] Stender M, Hoffmann N, Papangelo A. The basin stability of bi-stable friction-excited oscillators. *Lubricants* **8**(12): 105 (2020)

[20] Hoffmann N, Fischer M, Allgaier R, Gaul L. A minimal model for studying properties of the mode-coupling type instability in friction induced oscillations. *Mech Res Commun* **29**(4): 197–205 (2002)

[21] Kruse S, Tiedemann M, Zeumer B, Reuss P, Hetzler H, Hoffmann N. The influence of joints on friction induced vibration in brake squeal. *J Sound Vib* **340**: 239–252 (2015)

[22] Hoffmann N, Gaul L. Effects of damping on mode-coupling instability in friction induced oscillations. *ZAMM-Angew Math Me* 83(8): 524–534 (2003)

[23] Guan D H, Huang J C. The method of feed-in energy on disc brake squeal. *J Sound Vib* **261**(2): 297–307 (2003)

[24] Brunetti J, Massi F, D'Ambrogio W, Berthier Y. A new instability index for unstable mode selection in squeal prediction by complex eigenvalue analysis. *J Sound Vib* **377**: 106–122 (2016)

[25] Zhang Z, Oberst S, Lai J C S. On the potential of uncertainty analysis for prediction of brake squeal propensity. *J Sound Vib* **377**: 123–132 (2016)

[26] Papangelo A, Ciavarella M, Hoffmann N. Subcritical bifurcation in a self-excited single-degree-of-freedom system with velocity weakening–strengthening friction law: Analytical results and comparison with experiments. *Nonlinear Dynam* **90**(3): 2037–2046 (2017)

[27] Zhang Q X, Yu Z, Liu H, Mo J L, Xiang Z Y, Zhu S, Jin W W. Analysis of friction-induced vibration and wear characteristics during high-speed train friction braking process. *Tribol Int* **196**: 109701 (2024)

[28] Oberst S, Lai J C S. Nonlinear transient and chaotic interactions in disc brake squeal. *J Sound Vib* **342**: 272–289 (2015)

[29] Massi F, Baillet L, Giannini O, Sestieri A. Brake squeal: Linear and nonlinear numerical approaches. *Mech Syst Signal Pr* **21**(6): 2374–2393 (2007)

[30] Sinou J J, Jézéquel L. The influence of damping on the limit cycles for a self-exciting mechanism. *J Sound Vib* **304**(3–5): 875–893 (2007)

[31] Brunetti J, Massi F, Saulot A, Renouf M, D'Ambrogio W. System dynamic instabilities induced by sliding contact: A numerical analysis with experimental validation. *Mech Syst Signal Pr* **58**: 70–86 (2015)

[32] Liu N Y, Ouyang H J. Friction-induced vibration considering multiple types of nonlinearities. *Nonlinear Dynam* **102**(4): 2057–2075 (2020)

[33] Brunetti J, Massi F, D'Ambrogio W, Berthier Y. Dynamic and energy analysis of frictional contact instabilities on a lumped system. *Meccanica* **50**(3): 633–647 (2015)

[34] Geier C, Hamdi S, Chancelier T, Dufrénoy P, Hoffmann N, Stender M. Machine learning-based state maps for complex dynamical systems: Applications to friction-excited brake system vibrations. *Nonlinear Dynam* **111**(24): 22137–22151 (2023)

[35] Liu N Y, Ouyang H J. Friction-induced vibration of a slider-on-rotating-disc system considering uniform and non-uniform friction characteristics with bi-stability. *Mech Syst Signal Pr* **164**: 108222 (2022)

[36] Sümer B, Eray T, Koç İ M. Alteration of friction force of a harmonically excited elastomeric pillar. *Tribol Int* **113**: 297–305 (2017)

[37] Li Z L, Ouyang H J, Gu Y T, Martelli S, Yang S Y, Wei H T, Wang W,

Wei R H. Non-stationary friction-induced vibration with multiple contact points. *Nonlinear Dynam* **111**(11): 9889–9917 (2023)

[38] Hochlenert D. Nonlinear stability analysis of a disk brake model. *Nonlinear Dynam* **58**(1): 63–73 (2009)

[39] Schwarzer D, Hetzler H, Seemann W. Bifurcation behavior of a 1DOF sliding friction oscillator. In: Proceedings in Applied Mathematics and Mechanics, 2006: 331–332.

[40] Saha A, Wahi P, Bhattacharya B. Characterization of friction force and nature of bifurcation from experiments on a single-degree-of-freedom system with friction-induced vibrations. *Tribol Int* **98**: 220–228 (2016)

[41] Tonazzi D, Passafiume M, Papangelo A, Hoffmann N, Massi F. Numerical and experimental analysis of the bi-stable state for frictional continuous system. *Nonlinear Dynam* **102**(3): 1361–1374 (2020)

[42] Papangelo A, Hoffmann N, Grolet A, Stender M, Ciavarella M. Multiple spatially localized dynamical states in friction-excited oscillator chains. *J Sound Vib* **417**: 56–64 (2018)

[43] Sun C D, Huang S Y, Tao Y, Duan Z Q, Han Q, Chen K, Kan Y J, Ni Z H, Wei Z Y, Zhang Y, et al. Phononic insights into sliding friction. *Friction* **13**(7): 9441043 (2025)

[44] Sun Z J, Ge P Y, Chen S H, Huang S C, Xu H W, Wang C, Han R, Zhang X S, Liu H X, Luo J B, et al. Friction tuning of interlayer exciton recombination in van der Waals heterostructures. *Adv Mater* **37**(29): 2502986 (2025)

[45] Lazzari A, Tonazzi D, Brunetti J, Saulot A, Massi F. Contact instability identification by phase shift on C/C friction materials. *Mech Syst Signal Pr* **171**: 108902 (2022)

[46] Giannini O, Akay A, Massi F. Experimental analysis of brake squeal noise on a laboratory brake setup. *J Sound Vib* **292**(1–2): 1–20 (2006)

Matteo Cattai obtained his B.S. degree in mechanical engineering in 2022 and M.S. degree in mechanical engineering in 2024 from Sapienza University of Rome. He is currently pursuing a Ph.D. degree in theoretical and applied mechanics from Sapienza University of Rome under the supervision of Prof. Francesco Massi. His research focuses on numerical analysis of contact dynamics in tribological applications.

清華大学出版社 Tsinghua University Press | SciOpen